Actuator Fault Tolerant Offshore Wind Turbine Load Mitigation Control

Yanhua Liu[a], Ron J Patton[b] and Shuo Shi[c,*]

[a]School of Electrical Engineering Shandong University Jinan 250061 China; y.liu@sdu.edu.cn
[b]Department of Engineering University of Hull Cottingham Road Hull HU6 7RX UK;r.j.patton@hull.ac.uk
[c]State Grid Shandong Electric Power Research Institute, Jinan 250000, China; shisure@163.com

ARTICLE INFO

Keywords:
Bayesian optimization
Fault tolerant control
Individual pitch control
Gaussian Process
Monte Carlo simulation
Offshore wind turbine

ABSTRACT

Offshore wind turbine (OWT) rotors have large diameters with flexible blade structures which are subject to asymmetrical loads caused by blade flapping and turbulent or unsteady wind flow. Rotor imbalance inevitably leads to enhanced fatigue of blade rotor hub and tower structures. Hence, to enhance the life of the OWT and maintain good power conversion the unbalanced loading requires a reliable mitigation strategy, typically using a combination of Individual Pitch Control (IPC) and Collective Pitch Control (CPC). Increased pitch motion resulting from IPC activity can increase the possibility of pitch actuator faults and the resulting load imbalance results in loss of power and enhanced fatigue. This has accelerated the emergence of new research areas combining IPC with the fault tolerant control (FTC)-based fault compensation, a so-called FTC and IPC "co-design" system. A related research challenge is the clear need to enhance the robustness of the FTC IPC "co-design" to some dynamic uncertainty and unwanted disturbance. In this work a Bayesian optimization-based pitch controller using Proportional-Integral (PI) control is proposed to improve pitch control robustness. This is achieved using a systematic search for optimal controller coefficients by evaluating a Gaussian process model between the designed objective function and the coefficients. The pitch actuator faults are estimated and compensated using a robust unknown input observer (UIO)-based FTC scheme. The robustness and effectiveness of this "co-design" scheme are verified using Monte Carlo simulations applied to the 5MW NREL FAST WT benchmark system. The results show clearly (a) the effectiveness of the load mitigation control for a wide range of wind loading conditions, (b) the effect of actuator faults on the load mitigation performance and (c) the recovery to normal load mitigation, subject to FTC action.

1. Introduction

The power rating of offshore wind turbines (OWTs) and the number of OWT farms are currently increasing worldwide to meet the growing demand for carbon-free energy [1]. With this demand there is clearly a need for OWTs to be more reliable and sustainable. This motivates the current work responding to two major challenges for sustainable operation of an OWT in Region 3 (full-load). The first challenge arises as unexpected OWT component faults lead to costly repairs and turbine down time, increasing operation and maintenance (O&M) costs and enhancing the levelized cost of energy. The probability of failure depends very much on the type of component. For example, pitch systems contribute approximately 22% of the annual turbine downtime second to malfunctions of the electrical subsystem [2]. Also pitch malfunctions can severely limit OWT operation and sustainability in Region 3, since the purpose of pitch control is to limit the power production to the rated value. The second challenge is that larger rotor blades and higher towers have resulted in enhanced asymmetrical blade loading due to wind turbulence, gravity, tower shadow, yaw misalignment, blade flexible dynamics [3], etc. The mitigation of these unbalanced loads requires advanced individual pitch control (IPC) in which the three pitch actuators work through individual control action, to compensate the rotating loads. Extensive studies describe the significance of IPC in wind turbines [4–10] and focus on validation of the use of IPC in realistic operating conditions [11–17]. Typically, the traditional collective pitch control (CPC) aims to maintain the rated generator power output, while the IPC system provides an additional pitch movement for each pitch actuator above the standard collective pitch motion with blade flapwise and edgewise loading knowledge. The approaches employed in aforementioned studies assume ideal sensing and actuation (i.e. conventional blade root strain gauges

*Corresponding author
ORCID(s): 0000-0002-4590-4658 (Y. Liu)

[8, 15, 16] or new fiber-optic strain sensors for blade root bending measurements [17]) and negligible variations in actuator dynamics.

However, sensors and actuators in the operation of wind turbines are known to be prone to potential faults, driving the emerging fields such as fault detection & diagnosis (FDD) and fault-tolerant control (FTC) for wind turbine faults ([18–24]). Fault estimation (FE) and compensation have proven to be powerful for minimizing the effects of unexpected faults, allowing wind turbine systems to tolerate performance degradation under certain abnormal situations [23]. A robust FE-based fault-tolerant controller using unknown input fuzzy observer [18] is built for a 4.8 MW wind turbine for generator torque actuator fault and rotor speed sensor fault against modelling errors and noises. An adaptive sliding observer-based FTC scheme [19] is proposed to estimate and compensate parametric pitch actuator faults with a baseline CPC controller. Similar fault-tolerant collective pitch controller with different wind turbine component faults is presented in [24].

However, compared to the conventional CPC controller, the additional pitch action from IPC is used to reduce blade loading without affecting the power output. The load reduction performance comes with much higher activities of pitch actuation from the IPC system, which in turn enhances the likelihood of pitch system faults. the existing FTC strategies require much higher activities of pitch actuation. The resulting pitch system faults cause a deterioration of the IPC load reduction performance because of increased pitch system activity. Therefore, designing both a reliable IPC controller and a FTC strategy (fault-tolerant IPC, FTIPC [20]) is of crucial importance to improve the reliability, safety, availability, and productiveness of OWTs. A combination of FTC with IPC becomes fundamental and aims to restore near-normal OWT function by alleviating the aerodynamic asymmetries and preventing faults from developing into serious failure, subsequent to faults that are considered incipient or not severe.

Nonetheless, the research involving IPC with FTC in the presence of faults is rarely considered. A passive fault-tolerant IPC scheme independent of the FDD and FTC process is proposed in the work [10], which presents a multivariable model-free adaptive control strategy with differential characteristic is constructed. However, passive FTC is relatively conservative and it cannot guarantee the system operates under reasonable performance due to the omission of possible fault types. There is a need to either (a) detect and isolate pitch faults whilst they are incipient (or small in effect), to inform the following operation and maintenance. If the faults are severe enough the machine can be shut-down before the faults become severe. Or (b) the pitch faults can be estimated on-line and then their effects compensated within each control loop using FTC. A fault diagnosis and accommodation technique for enabling or disabling the IPC according to the fault detection result of the azimuth angle sensor is proposed by [25]. [20] proposed a FDD with automatic signal correction system for detection and diagnosis of pitch actuator faults with an adaptive Proportional-Integral PI-based IPC algorithm, where the system robustness is verified by Monte Carlo simulation. However, the adaptive PI-based IPC algorithm is model-based which still suffers from an issue of robustness due to model-plant mismatch. A fault detection and diagnosis (FDD) and automatic signal correction algorithm for a pitch actuator fault within an IPC is proposed in [26] which focuses on one hydraulic oil leak fault (leading to pressure drop). However, this uses an FDD-based FTC which is complex to implement in a real system since the uncertainty in detection involves a detection delay combined with a delay in switching to a healthy redundant control system. The work in [26] is an FTC system based on FDD which can be considered an unrealistic way to achieve good FTC performance [27].

As an alternative to residual-based FDD, the FE strategy can be used that estimates both the fault effects and the pitch system states. Root bending sensor faults can be detected online through the model-based estimation of first-harmonic blade load signal with the wind data from a LiDAR system applied to the IPC system [28]. A fault-tolerant individual pitch control scheme is proposed to accommodate pitch actuator-related faults and attain the load mitigation performance in the faulty case based on a subspace predictive repetitive control approach [21]. The work presented in [29] describes a fault-tolerant IPC strategy against the pitch actuator fault using an adaptive sliding mode observer to provide a compensating controller with the fault estimates. The work in [30] proposes an LQR-based IPC strategy for simultaneous blade & tower loading mitigation in which the robust fault estimation (FE) is achieved using an unknown input observer (UIO), considering four different pitch sensor faults. However, the aforementioned studies except the work [20] fail to discuss and verify the system robustness, a significant problem for WT load mitigation, especially considering turbulence and changing wind conditions.

Above all, the present study is instructive for developing a robust active fault-tolerant individual pitch controller, promising to advance the state-of-the-art FTIPC field. The first contribution is to design a data-efficient Bayesian optimization BO-based PI pitch controller for output power and load reduction control while maintaining the extra pitch angle fluctuations as small as possible. The industry standard of PI CPC&IPC control is adopted with the PI

gains tuned using the data-efficient BO algorithm, without a requirement for model-based robustness. The algorithm computes the maximum of expensive objective functions [31], using Gaussian process (GP) kernel-based machine learning [32]. The second contribution is designing a UIO-based FTC scheme for different pitch actuator faults without affecting the nominal performance of pitch control under fault-free operation. This feature is very promising in terms of industry acceptance and validation. The paper also contributes a thorough robustness analysis using Monte Carlo simulation, based on a wide range of tabulated wind loading conditions. This whole study uses the NREL 5MW WT FAST simulator [33] with the inclusion of actuator dynamics and the simulation of actuator faults.

The work has led to the conclusion that the scenario of asymmetrical load reduction is analogous to FTC because the action of rotor bending (caused by wind loading) can itself be considered as a fault effect, to be compensated as a fault. One can recall that a fault acting in a system is an unwanted effect causing a performance deterioration and this is precisely what happens with rotor blade bending. It is interesting to consider "fault effects" acting in the pitch actuation and rotor blade systems i.e. actuator faults and bending moment effects. So, adverse root-bending moment variations can be considered as faults, or alternatively the measurements of the rotor bending can be considered to suffer from sensor faults. Another interesting principle is that the rotor system has a natural triplex dissimilar actuator redundancy which is necessary for the accommodation for the fault or imbalance effect. The three actuators play a dissimilar redundancy role since they are displaced by positions separated by 120 degrees around the rotor hub.

The remainder of the paper is organised as follows. Section 2 shows the design of a Bayesian optimization-based CPC & IPC PI pitch system using a GP model. Section 3 explains briefly the concept of the "co-design" strategy containing the combined PI-based IPC and FE-based FTC scheme. Section 4 describes the Monte Carlo simulation results used to evaluate and validate the effectiveness and robustness of the proposed strategy. Finally, load mitigation results including pitch actuation faults and the action of the FTC system in restoring "normal IPC" mitigation are shown for the chosen loading conditions. The results are given both in the time and frequency-domains. Some conclusions are provided in Section 5.

2. Problem Formulation

The major aim of this work is to combine FE-based FTC techniques with load mitigation controller for OWs through integrated co-design, illustrated in Fig.1. This actuator fault tolerant wind turbine load mitigation control strategy contains two parts: (a) a sustainable pitch controller specifically using the PI-based IPC technique to reduce the blade imbalance in Region 3 and (b) enhancing the fault-tolerance of proposed load mitigation method in the pitch actuator faulty case with unknown input observer UIO-based FTC. Therefore, the sustainability and reliability of OWTs are enhanced, thus reducing the operating cost. It is worth noting that the load information denotes the blade flapwise bending moments, which are assumed to provided by the conventional blade root strain gauges [8, 15, 16] or new fiber-optic strain sensors for blade root bending measurements [17].

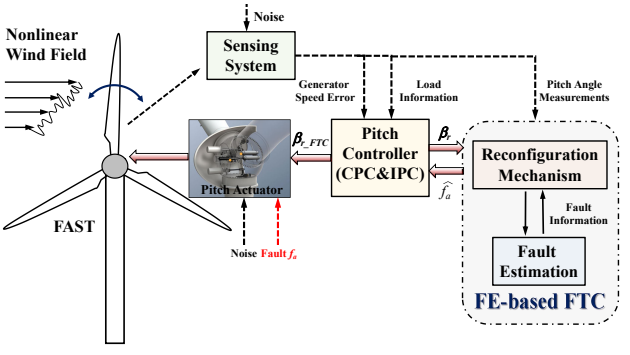

Figure 1: Proposed actuator fault tolerant wind turbine load mitigation control scheme

2.1. Baseline Pitch Control System

The FAST NREL 5MW reference turbine is adopted as the offshore wind turbine benchmark model for synthesis and evaluation of the fault-tolerant IPC scheme. FAST is a nonlinear aero-elastic structural-dynamic model developed

by the NREL of the USA for three-bladed horizontal axis wind turbines [33]. The pitch control becomes important in Region 3 and the pitch angles are regulated (from 0 degree) to constrain the generator power output [34]. This is important to keep the turbine from the excessive loading and damage. Because FAST does not include the pitch dynamics, a hydraulic pitch system is adopted and considered in this paper. For large offshore wind turbines suffering from extreme aerodynamic loading, hydraulic pitch systems are considered easy-maintenance and fail-safe. Here, each hydraulic pitch actuator is modelled as a linear closed-loop second order system. In Region 3, a gain-scheduling proportional-integral (PI) pitch controller is adopted as the CPC to change three pitch angles simultaneously, illustrated in (1).

$$\triangle\beta_r(t) = GK(\beta)(K_{p_{CPC}}(t) \triangle w(t) + K_{i_{CPC}}(t) \int_0^t \triangle w(t)dt) \tag{1}$$

where $\triangle\beta_r$ denotes small perturbations of the pitch angle reference around the operating condition. $\triangle w$ denotes the error between the rated generator speed set value and the corresponding measurement. $K_{p_{CPC}}$, $K_{i_{CPC}}$ represent the proportional and integral gains. The gain correction factor $GK(\theta)$ is to adjust the values of K_p, K_I with respect to the time-varying wind speed because the sensitivity between the aerodynamic power and blade pitch angle has a nonlinear characteristic over Region 3.

An extra pitch angle generated by the designed PI-based IPC system (i.e. Eq.2) is then added to the collective pitch angles individually in order to mitigate the blade unbalanced loading. Two single-input-single-output pitch control loops with the same PI parameter values are designed for the main-bearing tilt and yaw moment compensation, as illustrated in Fig.2. In this work, additional pitch angle variations from the IPC system typically have frequencies of more than 0.1Hz for the studied wind turbine model. The corresponding frequencies of the collective pitch angles from the CPC are less than 0.1Hz. In this sense, the IPC strategy is decoupled from the CPC system, thereby avoiding the impact of additional introduced pitch angles on generator power instability. The interested reader should refer to the earlier literature [35] for further details of the IPC strategy used. In most studies, the PI controller parameters of the CPC and IPC systems $K_{p_{CPC}}, K_{i_{CPC}}, K_{p_{IPC}}, K_{i_{IPC}}$ are usually tuned manually by trial and error [4], and this is considered inefficient and cannot guarantee robust or optimal performance. Therefore, it is fundamental to find an appropriate method to improve the performance of the PI-based CPC and IPC controllers.

$$C_{PI-IPC}(s) = K_{p_i} + \frac{K_{i_{IPC}}}{} \tag{2}$$

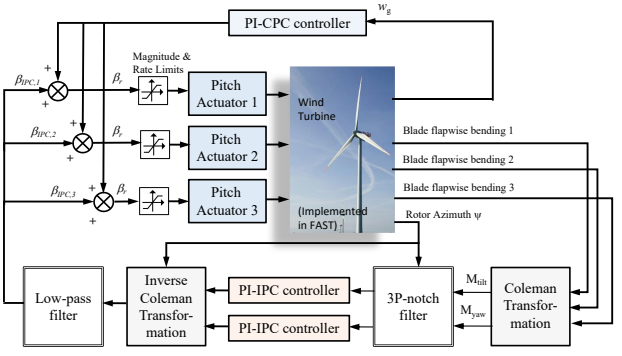

Figure 2: The designed IPC system for load mitigation [29]

2.2. Bayesian Optimization-based Pitch Controller

Data-driven and learning-based control methods provide interesting alternatives due to their nonlinear function approximation and optimization abilities. The optimization algorithm adopted here is Bayesian optimization (BO), which is data-efficient in computing the maximum of expensive objective functions [31]. The BO uses Gaussian process

(GP) machine learning to establish a *surrogate* for the objective function and quantify the uncertainty in the *surrogate*. The algorithm then uses the acquisition function defined from the *surrogate* to decide where to sample the data [36]. GP regression is a popular kernel-based learning approach with good potential to analyse implicit patterns between a series of training datasets [32]. The GP method provides the advantages of modelling flexibility, uncertainty estimation as well as learning smoothness and noise parameters from a training dataset [37]. The BO approach is applicable for situations where the closed-form mathematical representation of the objective function is unknown, but the noisy function observations can be achieved.

The above description outlines the model-free optimization method for both the PI-based CPC and IPC systems using the BO technique. The BO algorithm directly searches for the optimal PI controller coefficients by evaluating the designed objective function (i.e. score) at the end of each simulation episode. The GP probabilistic model is adopted to map the relationship between the PI-based CPC & IPC controller coefficients and the proposed objective criterion. In the GP model, the uncertainty is normally small near the observation value, and becomes large when it is far away from the observation value. The GP model describes the favourable attributes of both estimates and predictions of the uncertainty bounds with respect to the objective functions.

Generally speaking, BO uses the GP model (or other *surrogate function*) to approximate the target function f. Moreover, the acquisition function is used to decide the next update of the PI controller coefficients x_{k+1} to be sampled and evaluated based on the GP model [36]. The x_{k+1} space of the GP model with high mean and high uncertainty is referred to as the promising regions for the next trial. Therefore, the computed decision of the next PI controller coefficients represents a trade-off between the exploration (areas with high uncertainty) and exploitation (areas close to the current optimal observation). The advantage of the BO algorithm is that a few evaluations are required to find the extrema of the objective functions with multiple local maxima (i.e. non-convex optimization). Hence, data efficiency is achieved by searching and fitting within the required regions, rather than exploring all of the objective function spaces. GP is a random process involving an infinite set of variables, any finite subsets of which are jointly Gaussian distributed. The *priori* statistics of a GP stochastic model $f(x)$ can be fully defined by a mean function $m(x)$ and a covariance function $k(x, x^\star)$:

$$\begin{aligned} f(x) &\sim \mathcal{GP}(m(x), k(x, x^\star)) \\ m(x) &= \mathbb{E}[f(x)] \\ k(x, x^\star) &= cov(f(x), f(x^\star)) \end{aligned} \tag{3}$$

where $x \in \mathbb{R}^D$ is the input vector, D is the dimension of inputs (denotes the dimension of PI parameters here), $f(x)$ and $f(x^\star)$ are arbitrary variables indexed by input pairs x and $x^\star$. Generally speaking, $k(x, x^\star)$ is usually referred to as a kernel function, which has various forms all parametrised by some specific hyperparameters $\boldsymbol{\theta}$ [32]. The covariance function describes the process behaviour and defines the proximity between arbitrary random points of the Gaussian function, which aims to achieve the forecast of value and uncertainty information for the unknown demand point from the training dataset [38]. In this study, the rational quadratic (RQ) kernel with automatic relevance determination (ARD) is selected as the covariance function:

$$\begin{aligned} k(x, x^\star) &= h_f^2[1 + \frac{1}{2\alpha} r^2(x, x^\star)]^{-\alpha} \\ r^2(x, x^\star) &= \sum_{d=1}^{D} \frac{1}{\lambda_d^2}(x_d - x_d^\star)^2 \end{aligned} \tag{4}$$

where h_f controls the output scales and λ_d controls the input scales in each d dimension, x_d denotes the d_{th} dimension variable of input vector x. $\alpha > 0$ means the shape parameter. The parameter λ_d determines the smoothness of the selected covariance function. The hyperparameter vector values $\boldsymbol{\theta} = [h_f, \alpha, \lambda_d]'$ can be achieved by the optimization of the log marginal likelihood function [32]:

$$\log p(y|\theta) = -\frac{1}{2}\log|K| - \frac{1}{2}y^T K^{-1} y - \frac{n}{2}\log(2\pi) \tag{5}$$

The hyperparameter optimization adopts gradient-based standard non-convex optimization algorithms [39]. In order to achieve the target forecast $f^\star$ for a new given input $X^\star$ from the trained *posterior* GP model, the extended joint distribution is expressed as follows:

$$\begin{bmatrix} f^\star \\ y \end{bmatrix} \sim \left(\begin{bmatrix} m(X^\star) \\ m(X) \end{bmatrix}, \begin{bmatrix} k(X^\star, X^\star) & k(X^\star, X) \\ k(X, X^\star) & K + \sigma^2 I \end{bmatrix} \right) \tag{6}$$

with $k(X^\star, X) = k(x, X^\star)^T = [k(x_1, X^\star), \cdots, k(x_N, X^\star)]$, $K = K(X, X) = [k(x_1, X), \cdots, k(x_N, X)]$, where input vector $X = [x_1, x_2, \cdots, x_N]'$, new input vector $X^\star = [x_1^\star, x_2^\star, \quad \cdots, x_N^\star]'$, y denotes the known output and N is the number of new inputs. With the optimized θ from maximizing (5), the above required covariance matrix can be achieved with (4). According to the joint Gaussian Distribution Theorem [32], the predicted result for the target is illustrated as:

$$\begin{aligned} \mu(f^\star) &= m(X^\star) + k(X^\star, X)[K + \sigma^2 I]^{-1}(Y - m(X)) \\ var(f^\star) &= k(X^\star, X^\star) - k(X^\star, X)[K + \sigma^2 I]^{-1} k(X, X^\star) \end{aligned} \tag{7}$$

For a given GP model, the acquisition function is used to provide an optimization search guide for the objective function optimum. In this study, the Gaussian process upper confidence bound (GP-UCB) method is adopted as the acquisition function [40], which is shown as follows:

$$\begin{aligned} a_{UCB}(x; \{X, y\}, \theta) &= \mu(x) + \sqrt{\eta \beta_m var^2(x)}, \\ \beta_m &= 2ln(DK^2\pi^2/(6\delta)) \end{aligned} \tag{8}$$

where m is the evaluation number, $\delta > 0$ is the probabilistic tolerance, var is variance of GP predictions, $\eta > 0$ is an adjustable positive conversion efficiency parameter, and β_m is the learning rate to obtain the optimal regression performance. The following acquisition function is used to determine which PI controller parameter values should be evaluated in the next step:

$$x_{m+1} = argmax_x a_{UCB}(x) \tag{9}$$

In this study, the aim is to determine the optimal PI controller coefficients for both the PI-based CPC and IPC to maximize this criterion. That is, CPC is used to reduce the generator power fluctuations and tower fore-aft/side-side bending moments. The IPC controller aims to mitigate the blade flapwise bending moments. Therefore, the objective function (score) used for optimizing the PI parameters is shown as (10), where std denotes the standard deviation.

$$\begin{aligned} Score_{CPC} &= \rho_1 std(error(Genspeed)) + \rho_2 std(towerfore) \\ &\quad + \rho_3 std(towerside) \\ Score_{IPC} &= \rho_4 std(bending1) + \rho_5 std(bending2)/100 \\ &\quad + \rho_6 std(bending3) \\ \text{with } \rho_1 &= 1, \rho_2 = 0.01, \rho_3 = 0.02, \rho_4 = \rho_5 = \rho_6 = 0.01 \end{aligned} \tag{10}$$

The block diagram of the proposed BO-based PI pitch controller is illustrated in Fig.3. The BO based on a GP model is used to update the PI-based CPC/IPC controller with a high possibility of increasing the rewards (criteria) and then collecting the new OWT performance (PI controller parameters and objective function evaluations) to enhance the GP model. Moreover, each optimization loop is carried out under the same wind condition. In this case, the relationship between rewards and PI parameters can be approximated by a GP model. By repeating this process, the GP model can iteratively approximate the real objective function in regions with potentially optimal performance. Eventually, the PI-based CPC/IPC controller learns the optimal controller coefficients by interacting directly with the OWT.

The flowchart of the tuning of the proposed pitch controller using the BO algorithm is shown in Fig.4, where x_0 is the vector of initial PI parameters $K_{p_{CPC}}, K_{i_{CPC}}, K_{p_{IPC}}, K_{i_{IPC}}$, f is the initial GP model between the criterion and the

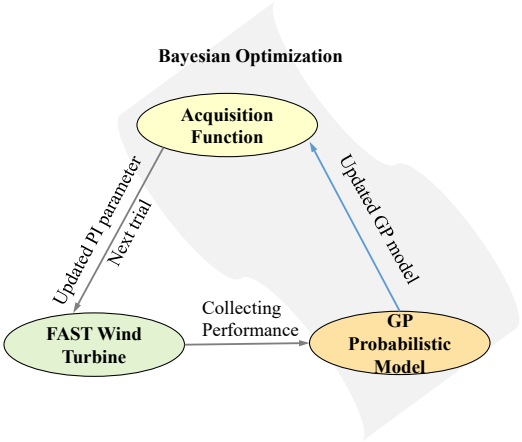

Figure 3: Bayesian optimization-based PI pitch controller

PI controller parameters. m is the optimization evaluation number, LB and UB are the set lower and upper bounds of the PI controller, respectively. According to the experiment, the evaluation time of each optimization loop is 300s. The stopping criteria denotes the evaluation number m is larger than the defined value or the score discrepancy is smaller than 0.001.

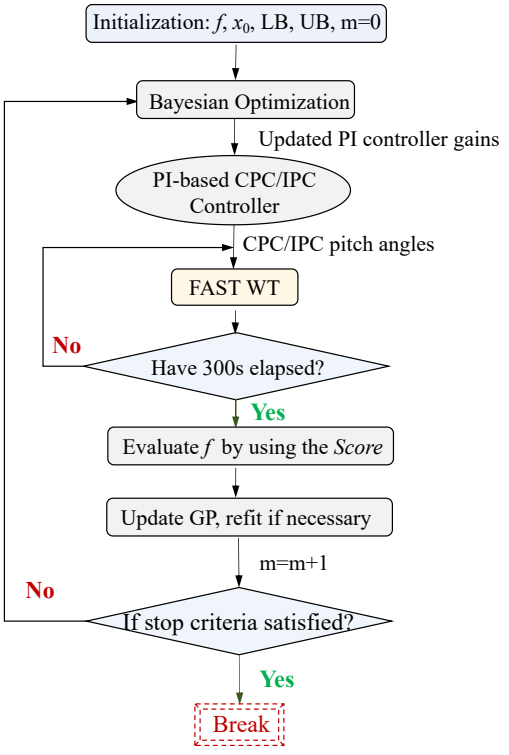

Figure 4: Flowchart of the PI-based CPC/IPC wind turbine pitch controller using BO algorithm

3. Pitch Actuator System Fault Modelling and FE-based FTC Design for Fault Compensation

3.1. Pitch Actuator System Fault Modelling

A hydraulic pitch actuator modelled as a closed-loop second order system [41] is applied in the NREL 5MW WT model to enable the actuator FE signals to be generated. The three pitch systems are assumed to have the same dynamics in the fault-free case, as shown in (11). Due to the physical system constraints, pitch angles and rates are restricted to [0,90]° and [-8,8]°/s in the simulation.

$$\frac{\beta}{\beta_r} = \frac{{w_{n_0}}^2}{s^2 + 2\xi_0 w_{n_0} s + {w_{n_0}}^2} \tag{11}$$

where ξ_0 and w_{n_0} are the nominal damping ratio and natural frequency parameters. β and β_r are the pitch actuator output and rated pitch angles, respectively. In this study, only pitch actuator-related fault are investigated including the pitch actuator initial faults with changing dynamics and loss of effectiveness, as illustrated in Fig.5. The following section will illustrate the faulty pitch system modelling.

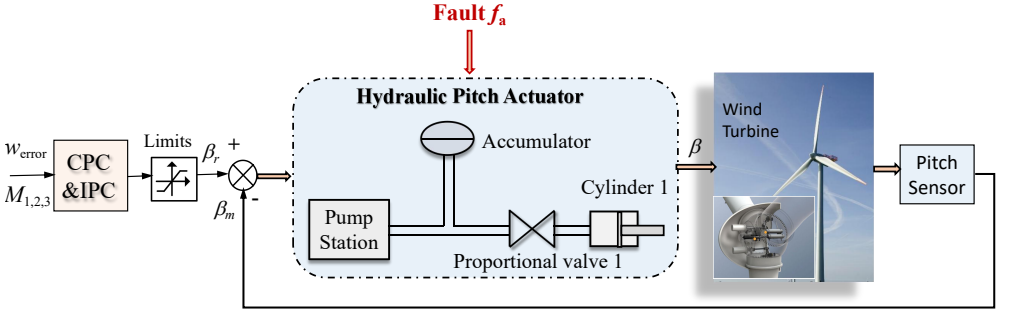

Figure 5: Wind turbine hydraulic pitch system with pitch actuator faults

3.1.1. Pitch Actuator Initial Faults with Changing Dynamics

Some potential hydraulic pitch system faults include the oil leakage due to oil seal failure or improper hydraulic fluid management, the pump damage resulting from continuous pump operation, as well as the high air content in oil, which are referred to as "pitch actuator initial faults with changing dynamics". This kind of fault itself requires manual off-line maintenance. If the pitch actuator dynamics change too much, the pitch system will not be able to pitch the corresponding blade to the desired position.

These will lead to the situation where the blade pitch system has changed dynamics (ξ_0, w_{n_0}), causing slow pitching performance and unstable turbine outputs. It will even lead to the "pitch actuator stuck fault (i.e. seized blade movement), requiring repair during turbine shut-down [42]. The faulty parameters can be modelled as convex combinations of $\xi_0 w_{n_0}$, $w_{n_0}^2$ and the fault level θ_f [29]:

$$\begin{aligned} w_n^2 &= w_{n_0}^2 + (w_{n_f}^2 - w_{n_0}^2)\theta_f \\ \xi w_n &= \xi_0 w_{n_0} + (\xi_f w_{n_f} - \xi_0 w_{n_0})\theta_f \end{aligned} \tag{12}$$

where ξ_f and w_{n_f} denote the dynamic parameters in the faulty case. The parameter $\theta_f \in [0, 1]$ indicates the fault level, where the larger the θ_f is, the more severe the actuator fault is. The corresponding dynamic parameters are illustrated in Table.1. From (12), the corresponding pitch actuator state-space model with initial fault f_a and unknown disturbance d and measurement noise d_s can be illustrated as (13), where D and D_s denote disturbance and sensor noise distribution matrices. β_m is the system output, that is, the measured pitch angles. F_a denotes the fault distribution matrix.

Table 1
Pitch system parameters

Fault type	Dynamic parameters	Reversible
Fault-free	$w_{n_0} = 11.11\ rad/s,\ \ \xi_0 = 0.6$	N/A
Hydraulic leakage	$w_{n_f} = 3.42\ rad/s,\ \ \xi_f = 0.9$	×
Pump wear	$w_{n_f} = 7.27\ rad/s,\ \ \xi_f = 0.75$	×
High air content	$w_{n_f} = 5.73\ rad/s,\ \ \xi_f = 0.45$	$\surd$

$$
\begin{aligned}
\begin{bmatrix} \dot{\beta} \\ \ddot{\beta} \end{bmatrix} &= \begin{bmatrix} 0 & 1 \\ -w_{n_0}^2 & -2\xi_0 w_{n_0} \end{bmatrix} \begin{bmatrix} \beta \\ \dot{\beta} \end{bmatrix} + \begin{bmatrix} 0 \\ w_{n_0}^2 \end{bmatrix} \beta_r \\
&\quad + F_a f_a + D d \\
\beta_m &= \begin{bmatrix} 1 & 0 \end{bmatrix} \begin{bmatrix} \beta \\ \dot{\beta} \end{bmatrix} + E_s d_s \\
f_a &= (1 - \frac{w_{n_f}^2}{w_{n_0}^2})(\beta - \beta_r)\theta_f + 2(\frac{\xi_0}{w_{n_0}} - \frac{\xi_f w_{n_f}}{w_{n_0}^2})\theta_f \dot{\beta} \\
F_a &= \begin{bmatrix} 0 \\ w_{n_0}^2 \end{bmatrix}
\end{aligned}
\tag{13}
$$

3.1.2. Pitch Actuator Loss of Effectiveness (LOSS)

Blade pitch actuators typically operate precisely to the pitch controller's reference (i.e. 100% effectiveness). However, the long-term operation of pitch actuators without proper maintenance will lead to changes in the pitch actuator dynamic response including faults with unknown or uncertain loss of effectiveness [43]. This partial loss of effectiveness fault (<100% effectiveness) means that the pitch actuators cannot achieve the pitch angle references from the CPC and IPC systems in a timely and accurate way. This generic actuator fault is normally caused by ageing internal components and leads to hydraulic leakage, clogging pumps or changes in dynamic parameter values. Hence, the performances of both the power regulation and blade load mitigation are degraded severely.

$$
\beta = \gamma * \frac{w_{n_0}^2}{s^2 + 2\xi w_{n_0} s + w_{n_0}^2} * \beta_r \tag{14}
$$

where $\gamma \in [0, 1]$ denotes the effectiveness level, $\gamma = 1$ means the actuator is 100% effective, $\gamma = 0$ is the total loss. The corresponding pitch actuator state-space model is illustrated in (15), where f_a is the pitch actuator LOSS fault. It can be concluded that Eq.(13) and Eq.(15) share the same format, thus the faulty pitch system can be presented by the same state-space model. Therefore, the proposed fault estimation-based FTC scheme can compensate for these two different pitch actuator faults.

$$
\begin{aligned}
\begin{bmatrix} \dot{\beta} \\ \ddot{\beta} \end{bmatrix} &= \begin{bmatrix} 0 & 1 \\ -w_{n_0}^2 & -2\xi_0 w_{n_0} \end{bmatrix} \begin{bmatrix} \beta \\ \dot{\beta} \end{bmatrix} + \begin{bmatrix} 0 \\ w_{n_0}^2 \end{bmatrix} \beta_r \\
&\quad + F_a f_a + Dd \\
\beta_m &= \begin{bmatrix} 1 & 0 \end{bmatrix} \begin{bmatrix} \beta \\ \dot{\beta} \end{bmatrix} + E_s d_s \\
f_a &= (\gamma - 1)\beta_r \\
F_a &= \begin{bmatrix} 0 \\ w_{n_0}^2 \end{bmatrix}
\end{aligned} \tag{15}
$$

The open-loop performance of one pitch actuator system in various faulty cases is evaluated and shown in Fig. 6.

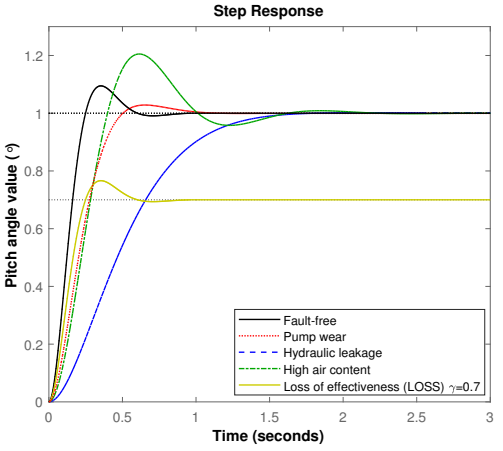

Figure 6: Step response of one pitch actuator system in different situations

Therefore, the linear representation of the faulty pitch system based on (13), and (15) can be expressed as:

$$
\begin{aligned}
\dot{x}_w &= Ax_w + Bu + F_a f_a + Dd \\
y &= Cx_w + E_s d_s
\end{aligned} \tag{16}
$$

where $x_w \in R^{n\times 1}$ and $u \in R^{m\times 1}$ represent the pitch system state matrix and control inputs, respectively. $y \in R^{p\times 1}$ denotes the system measurements. $d \in R^{l\times 1}$ means a combined effect of unknown disturbance and modelling uncertainty. $f_a \in R^{s\times 1}, F_a \in R^{n\times s}$ are the assumed actuator faults and fault distribution matrices. $E_s \in R^{p\times r}$ and $d_s \in R^{r\times 1}$ are the assumed measurement noise and sensor noise distribution matrices. The constant system matrices $A \in R^{n\times n},\ B \in R^{n\times m},\ D \in R^{n\times l},\ C \in R^{p\times n}$ are known with $n = 6,\ m = 3,\ l = 6,\ p = 3,\ s = 3\ , r = 3$.

3.2. FE-based FTC Design for Fault Compensation

3.2.1. UIO-based FE design

To obtain the actuator fault estimation, the fault f_a is modelled as an additional state component in the UIO error dynamics and the first order derivative of the actuator faults $\dot{f}_a$ is augmented as a disturbance, thus completing the augmented (state & fault) linear pitch system model given by:

$$\begin{aligned}\dot{\bar{x}} &= \bar{A}\bar{x} + \bar{B}u + \bar{D}\bar{d}\\ y &= \bar{C}\bar{x} + E_s d_s\end{aligned} \tag{17}$$

$$\bar{A} = \begin{bmatrix} A & F_a \\ \mathbf{0} & \mathbf{0} \end{bmatrix}, \bar{B} = \begin{bmatrix} B \\ \mathbf{0} \end{bmatrix}, \bar{D} = \begin{bmatrix} D & \mathbf{0} \\ \mathbf{0} & I \end{bmatrix}, \bar{C} = \begin{bmatrix} C & \mathbf{0} \end{bmatrix},$$
$$\bar{x} = \begin{bmatrix} x_w \\ f_a \end{bmatrix}, \bar{d} = \begin{bmatrix} d \\ \dot{f}_a \end{bmatrix}$$

where $\bar{x} \in R^{(n+s)\times 1}$, $\bar{d} \in R^{(l+s)\times 1}$ and $\bar{A} \in R^{(n+s)\times(n+s)}$, $\bar{B} \in R^{(n+s)\times m}$, $\bar{D} \in R^{n\times(l+s)}$, $\bar{C} \in R^{p\times(n+s)}$.

The following Assumptions and Lemmas illustrated in the Appendix form the basis for the robust UIO-based FTC design. On satisfying the Assumptions, the following UIO system [44] is proposed to estimate $\bar{x}$:

$$\begin{aligned}\dot{z} &= Mz + G\bar{B}u + Ly\\ \hat{\bar{x}} &= z + Hy\end{aligned} \tag{18}$$

where $z \in R^{(n+s)\times 1}$ denotes the observer states, and $\hat{\bar{x}} \in R^{(n+s)\times 1}$ is the estimate of $\bar{x}$. The designed matrices $M \in R^{(n+s)\times(n+s)}$, $G \in R^{(n+s)\times(n+s)}$, $L \in R^{(n+s)\times p}$ and $H \in R^{(n+s)\times p}$ are of appropriate dimensions.

The estimation error state is $e_x = \bar{x} - \hat{\bar{x}}$, with dynamics:

$$\begin{aligned}\dot{e}_x =&\ \dot{\bar{x}} - \dot{\hat{\bar{x}}}\\ =&\ (\Xi\bar{A} - L_1\bar{C})e_x + \Theta_1 z + \Theta_2 y + \Theta_3 u\\ &+\ \Xi\bar{D}\bar{d} - L_1 E_s d_s - H E_s \dot{d}_s\\ e_y =&\ \bar{C}e_x + E_s d_s\end{aligned} \tag{19}$$

$$\begin{aligned}&\Xi = I_{n+s} - H\bar{C}, L = L_1 + L_2, \Theta_1 = \Xi\bar{A} - L_1\bar{C} - M\\ &\Theta_2 = (\Xi\bar{A} - L_1\bar{C})H - L_2, \Theta_3 = (\Xi - G)\bar{B}\end{aligned} \tag{20}$$

To guarantee asymptotic stability of system (19), it is further assumed that the following conditions are satisfied:

$$\text{M is Hurwitz, } \textit{and} \ :\ \ \Theta_1 = 0,\ \ \Theta_2 = 0,\ \ \Xi - G = 0 \tag{21}$$

By satisfying (20)-(21), the error system (19) becomes:

$$\begin{aligned}\dot{e}_x &= (\Xi\bar{A} - L_1\bar{C})e_x + \Xi\bar{D}\bar{d} - L_1 E_s d_s - H E_s \dot{d}_s\\ e_y &= \bar{C}e_x + E_s d_s\end{aligned} \tag{22}$$

The term $\Xi\bar{D}\bar{d} - L_1 E_s d_s - H E_s \dot{d}_s$ indicates the effects of system disturbance and measurement noise acting on the UIO error dynamics (22). These uncertainties limit the accuracy of the UIO system state and fault estimates. Hence, the augmented observer (18) is required to be both stable and a robust UIO system with e_x converging asymptotically to zero in finite time. This requires all the eigenvalues of M to be assigned to the left half of the complex plane. Here, the effects of uncertainties are attenuated using H_∞ optimization [27].

Theorem 1. If there exist a symmetric positive definite matrix $P \in \mathbb{R}^{(n+s)\times(n+s)}$ and appropriate matrices $M_1 \in \mathbb{R}^{(n+s)\times s}$ and $M_2 \in \mathbb{R}^{(n+s)\times s}$, the error system (22) is robustly stable with H_∞ performance satisfying $\|G_{e_x\bar{d}}\|_\infty < \lambda$ for any disturbance $w_d \in \mathcal{L}_2(0,\infty)$ and a specific constant parameter λ. Thus, one sufficient condition is:

$$\begin{bmatrix} \Delta_{11} & (P - M_1\bar{C})\bar{D} & -M_2E_s + \bar{C}^T E_s & -M_1E_s & \bar{C}^T \\ \star & -\lambda^2 I & 0 & 0 & 0 \\ \star & \star & E_s^T E_s - \lambda^2 I & 0 & 0 \\ \star & \star & \star & -\lambda^2 I & 0 \\ \star & \star & \star & \star & -I \end{bmatrix} < 0 \tag{23}$$

where $\Delta_{11} = He(P\bar{A} - M_1\bar{C}\bar{A} - M_2\bar{C})$, with $He(X) = X + X^T$. $M_1 = PH$, $M_2 = PL_1$. The disturbance matrix is $w_d = [\bar{d}\ d_s\ \dot{d}_s]^T$. Theorem 1 can be proved jointly by *Lemma 1* and the Schur Complement Theorem [45].

On satisfying the LMI (23), the availability of the designed UIO with stable error dynamics is guaranteed. However, e_x will further affect the closed-loop system transient performance, which can be attenuated if the observer dynamics are designed to be much faster than the closed-loop system dynamics. Therefore, a pole placement constraint introduced in *Lemma 2* is used to place the eigenvalues of matrix M within a suitable vertical strip region.

Remark 1. *The observer eigenvalues (22) can be placed to the vertical region $\mathcal{D} : a < Re(\eta) < b$ with given negative scalars a and b ($a < b < 0$), such that:*

$$\begin{bmatrix} 2\Delta_{11} - 2bP & 0 \\ \star & -2\Delta_{11} + 2aP \end{bmatrix} < 0 \tag{24}$$

A positive constant λ together with negative parameters a,b are selected appropriately. By solving the LMIs (23) and (24), P, M_1, M_2 can be achieved. Furthermore, the matrices L_1 and H are obtained with $H = P^{-1}M_1$, $L_1 = P^{-1}M_2$. Thus M, G, H and L can be achieved subsequently from (20)-(21). The actuator fault estimation $\hat{f}_a$ can thus be achieved by the designed UIO system.

3.2.2. FTC design

Given that the actuator fault is matched to the control channel (Assumption 1 satisfied), the pitch actuator fault can be compensated directly using a straightforward strategy to achieve fault-tolerance, whereby the reconstructed faults are subtracted from the pitch control reference:

$$\beta_{r\_FTC} = \beta_{rf} - \hat{f}_a \tag{25}$$

Moreover, $\hat{f}_a$ is set to zero in the first 10s of the simulation to avoid feeding back the initial transients. After applying the correction (25), the pitch system with FTC is:

$$\begin{aligned} \dot{x}_w &= Ax_w + B(u - \hat{f}_a) + F_a f_a + Dd \\ y &= Cx_w \end{aligned} \tag{26}$$

It can be seen clearly from the above that the modification parameter has the value $k = 1$ in the fault-free case. The compensating controller is active if and only if a fault f_a happens. The performance of the proposed FTC system depends on the accuracy of the FE action. Therefore, the proposed FTC controller (26) can compensate the faults effectively which enables the faulty pitch system operates as a normal pitch system. Hence, according to the above discussion, the BO-based PI pitch controller scheme is proposed, as shown in Fig.7 consisting of: (a) BO-designed PI controllers (CPC & IPC), where the PI-IPC makes use of the Coleman Transformation based scheme (see [5, 30]) and the pitch angle & rate constraints are applied; (b) (UIO design with H_∞ optimization) FE-based FTC considering the pitch actuator fault.

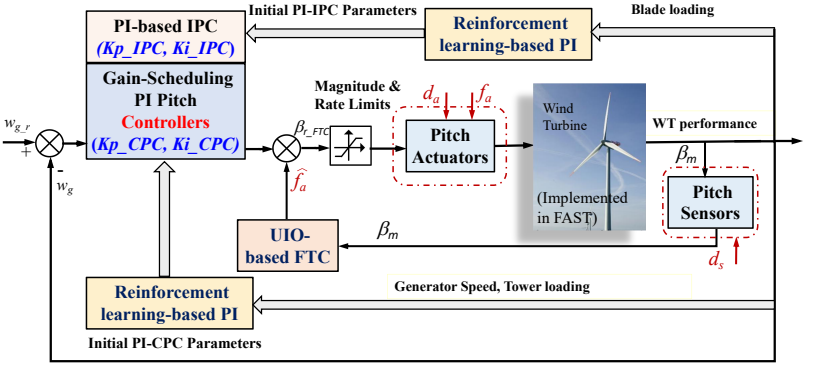

Figure 7: Proposed Bayesian optimization-based WT pitch controller and fault-tolerant IPC "co-design" scheme

Table 2
Verified wind conditions (WCs)

Load Case	MWS	TI	WS	Load Case	MWS	TI	WS
L18_1	18m/s	0.204	0.049	L21_1	21m/s	0.126	0.122
L18_2	18m/s	0.032	0.093	L21_2	21m/s	0.122	0.200
L18_3	18m/s	0.158	0.050	L21_3	21m/s	0.199	0.117
L18_4	18m/s	0.024	0.181	L21_4	21m/s	0.088	0.243
L18_5	18m/s	0.070	0.079	L21_5	21m/s	0.112	0.145
L18_6	18m/s	0.137	0.196	L21_6	21m/s	0.210	0.103
L18_7	18m/s	0.039	0.135	L21_7	21m/s	0.011	0.125
L18_8	18m/s	0.243	0.025	L21_8	21m/s	0.197	0.040
L18_9	18m/s	0.200	0.046	L21_9	21m/s	0.047	0.296
L18_10	18m/s	0.035	0.248	L21_10	21m/s	0.167	0.259
L18_11	18m/s	0.105	0.162	L21_11	21m/s	0.147	0.117
L18_12	18m/s	0.198	0.023	L21_12	21m/s	0.169	0.136
L18_13	18m/s	0.188	0.234	L21_13	21m/s	0.090	0.074
L18_14	18m/s	0.204	0.246	L21_14	21m/s	0.155	0.235
L18_15	18m/s	0.208	0.089	L21_15	21m/s	0.149	0.292
L18_16	18m/s	0.146	0.111	L21_16	21m/s	0.005	0.274
L18_17	18m/s	0.142	0.153	L21_17	21m/s	0.021	0.167
L18_18	18m/s	0.133	0.146	L21_18	21m/s	0.167	0.057
L18_19	18m/s	0.154	0.194	L21_19	21m/s	0.163	0.045
L18_20	18m/s	0.146	0.223	L21_20	21m/s	0.058	0.270

4. Simulation Results

The effectiveness of the proposed BO-based fault-tolerant IPC is illustrated through a series of case studies using the NREL FAST 5MW offshore wind turbine [33]. The full-field turbulent wind speed is generated by the NREL TurbSim software[46]. The robustness and reliability are investigated via extensive Monte Carlo simulations. In total, 40 wind conditions have been carried out by considering different wind profiles with mean hub-height wind speed (MWS) 18 & 21 m/s, turbulence intensity (TI) within [0,0.25] and wind shear (WS) within [0,0.3], as shown in Table 2 and Fig.8. Each simulation loop lasts for 1000s and the simulation sampling interval is 0.0125s.

The Monte-Carlo simulation results aim to (a) illustrate the proposed BO-based load mitigation controller performance for a wide range of wind loading conditions in the fault-free case, (b) investigate the actuator fault effects on the load mitigation performance and the recovery to normal load mitigation subject to FTC action in the both one-fault and multi-fault case. In order to analyze the results clearly, the different simulation scenarios are defined with name abbreviations. Table.3 explains the defined names at the hub-height wind speed of 18m/s, where f denotes pitch

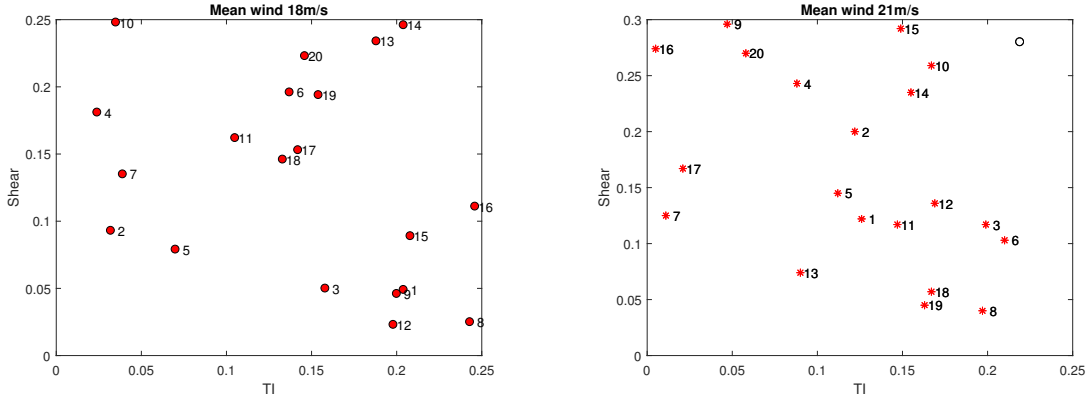

(a) Mean wind speed 18m/s (b) Mean wind speed 21m/s

Figure 8: The distribution of verified wind conditions

Table 3
Wind turbine performance comparison results under various conditions

Name	Baseline System	Compared System
18CPC_PIVS	Old PI-CPC (no f no FTC)	New PI-CPC (no f no FTC)
18IPC_PIVS	Old PI-IPC (no f no FTC)	New PI-IPC (no f no FTC)
18CPC_fault	New PI-CPC (no f no FTC)	New PI-CPC (with f no FTC)
18IPC_fault	New PI-IPC (no f no FTC)	New PI-IPC (with f no FTC)
18CPC_FTC	New PI-CPC (with f no FTC)	New PI-CPC (with f & FTC)
18IPC_FTC	New PI-IPC (with f no FTC)	New PI-IPC (with f & FTC)

actuator fault. Similar explanations follow for the other cases under hub-height wind speed of 21m/s. A defined name ends with "_PIVS" reflects the effectiveness of designed Bayesian optimization-based PI scheme. A defined name ends with "_fault" shows the effects of considered pitch actuator faults on WT performance. A defined name ends with "_FTC" reflects the effectiveness and robustness of designed fault-tolerant IPC scheme using BO algorithm. A defined name with "CPC" represents the pitch system contains only the CPC controller. A defined name with "IPC" indicates that the pitch system consists of the CPC and IPC controller.

The performance comparison = (Considered OWT performance − Original OWT performance)/ Original OWT performance is adopted here. The considered OWT performance denotes the standard deviations (STD) of generator power fluctuation, blade flapwise bending 1&2&3, main bearing tilt/yaw moment, tower fore-aft/side-side bending moment and pitch angles/rates. The considered OWT performance is under the "baseline system" shown in Table. 3. The original OWT performance is under the "compared system"in Table. 3. Note that, the lower the performance the better the optimization performance is achieved.

4.1. Fault-free Case

Two BO-optimization loops of IPC and CPC are implemented to obtain optimal parameters $K_{p_{CPC}}$, $K_{i_{CPC}}$, $K_{p_{IPC}}$, $K_{i_{IPC}}$ under the wind condition with hub-height 21m/s, 0.219 TI, 0.280 shear (i.e. high wind speed, high TI and high shear) in the fault-free case. Firstly, the BO loop for achieving the best controller parameters of PI-based CPC is executed. Then the BO loop for the PI-based IPC is performed on the basis of the optimal CPC parameters. The related optimization settings and optimization results of the two BO loops are represented in Table.4. The initial starting points of BO loops are the original parameters of the CPC and IPC controllers obtained by manual tuning. For the system functional safety, the upper & lower bounds of the PI parameters are restricted to a small range.

The changes of $K_{p_{CPC}}$, $K_{i_{CPC}}$, $K_{p_{IPC}}$, $K_{i_{IPC}}$ with the iteration number during the BO process are shown in Fig.9, where the first subplot represents the change in score. Note that the corresponding PI parameters with the smallest evaluation score are the optimal case. For the PI-based CPC optimization loop, the original score using (10) decreases

Table 4
Settings and results of two BO loops

Step 1: PI-based CPC BO loop	
Starting point	$x_0 = [0.01882861 \quad 0.008068634]$
Lower bounds	$LB = [0.01 \quad 0.003]$
Upper bounds	$UB = [0.08 \quad 0.02]$
Iteration number	$m = 40$
Results	$K_{p_{CPC}} = 0.065313, \quad K_{i_{CPC}} = 0.011674$
Step 2: PI-based IPC BO loop	
Starting point	$x_0 = [0.00002 \quad 0.00001]$
Lower bounds	$LB = [0.000005 \quad 0.000001]$
Upper bounds	$UB = [0.00006 \quad 0.00003]$
Iteration number	$m = 40$
Results	$K_{p_{IPC}} = 0.000016959, \quad K_{i_{IPC}} = 0.000002469$

from 482.83 to 283.3, as illustrated in Fig.9 (a). For the PI-based IPC BO loop, the original score decreases from 71.74 to 69.46, shown in Fig.9 (b). It is important to note that the CPC loop score has been improved substantially within the lower and upper settings of PI parameters, and this is reflected in the generator power fluctuation mitigation.

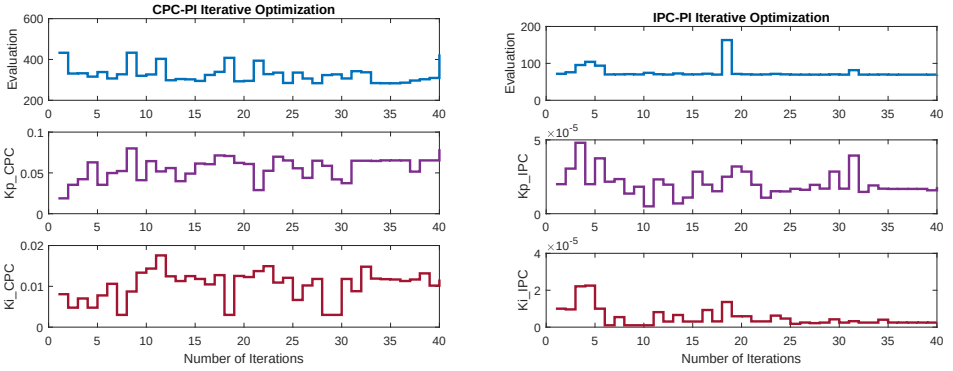

(a) CPC system (b) IPC system

Figure 9: Bayesian optimization-based PI pitch controller

Fig.10 shows the Monte Carlo simulation results with updated PI-based CPC & IPC under 40 wind conditions with hub-height wind speed 18m/s and 21m/s in the fault-free case. The central marks in the boxes indicates the median values. The box bottom and top edges indicate the 25th & 75th percentiles. The whiskers extend to the extreme data points not considered as outliers. The outliers are plotted individually using '+' symbol.

It can be seen that the designed BO-based PI controller can decrease the generator power fluctuation around -45%, blade flapwise bending moment fluctuation nearly -10%, the tower fore-aft bending -20% under CPC or IPC case. Moreover, the tower side-side bending is reduced -10% in the IPC case but enhanced slightly for CPC. This is because the tower side-side bending is mainly controlled by the generator torque. The main-bearing tilt/yaw moment is not affected too much in this case. The pitch angle and pitch rate fluctuations are mitigated in the IPC case, which means the updated IPC controller can achieve better wind turbine performance with less pitch movements. The alleviation of pitch activities turns out to be quite important to reduce the increased risk of pitch actuator cyclic fatigue failure in the IPC case.

4.2. One-fault Case

Here, it is assumed that only one pitch actuator is subjected to the studied pitch actuator fault and the BO-based PI CPC &IPC are used in all considered cases. Pitch actuator 1 is considered to suffer from the pitch actuator initial faults with changing dynamics during [200,1000]s. Pitch actuator 2 is assumed to suffer from the pitch actuator loss

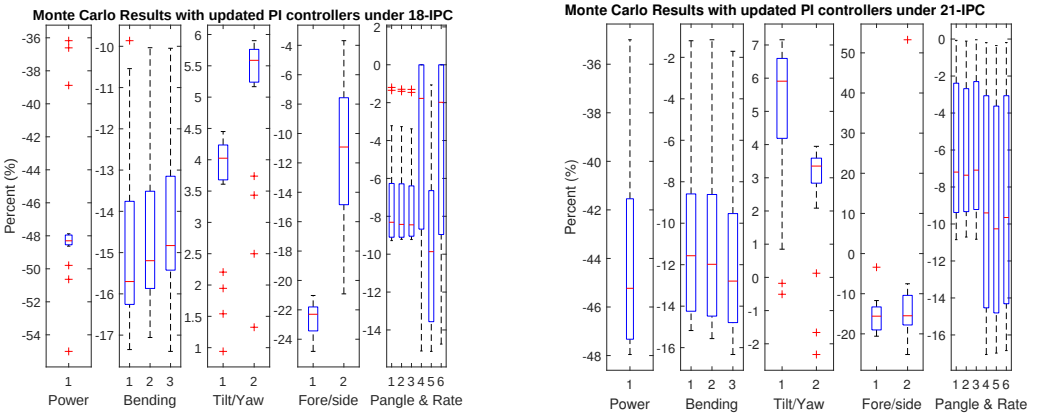

(a) WT performance under mean wind speed 18m/s (b) WT performance under mean wind speed 21m/s

Figure 10: Wind turbine performance with updated PI-based CPC & IPC in the fault-free case

of effectiveness fault during [600,1000]s. In order to demonstrate the fault effects, the fault detection & estimation and the FTC performance, the following results are presented and analyzed: (a) Monte Carlo simulation results with pitch actuator suffering from one single fault; (b) the FE result.

The Monte Carlo simulation results for single pitch high air content fault and single pitch actuator loss of effectiveness fault are depicted in Fig.11 and Fig.12, respectively. It can be discerned that the power fluctuation and the load performance present different levels of increases, especially in the case with pitch actuator LOSS fault. The faulty blade flapwise bending moment shows larger fluctuation t than the corresponding root-bending of the other two blades with the healthy pitch actuators. To be more specific, the flapwise bending 1 presents 28.9% enhancement while flapwise bending moments of actuators 2 and 3 only have 8.9% and 5.3% enhancement in mean value, as shown in Fig.11. Similarly, the flapwise bending 2 presents 36.7% enhancement while flapwise bending 1 and 3 only have 23.1% and 7.7% enhancement in mean value in Fig.12. The enhanced aerodynamic asymmetries on the rotor lead to an increase in main bearing tilt and yaw moment. Due to the couplings between the blades and the tower, the tower fore-aft and side-side moments presents significant enhancement. Moreover, it is interesting to note that the healthy pitch actuators move more frequently to recover the negative fault effect. That is, Fig.11 shows that the pitch rates of actuators 2 and 3 are higher than pitch rate of actuator 1 while Fig.12 illustrates the pitch rates of actuators 1 and 3 are higher than pitch rate of actuator 2. It is important to notice that the designed FTC can compensate the fault effects.

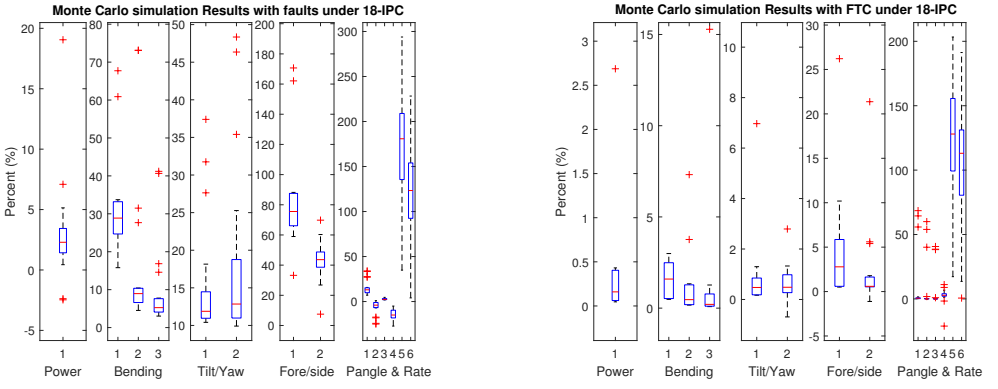

(a) With single pitch high air content fault (no FTC). (b) With single pitch high air content fault (with FTC).

Figure 11: Monte Carlo simulation results under 20 wind conditions with hub-height wind speed 18m/s with pitch actuator 1 suffering from the high air content fault

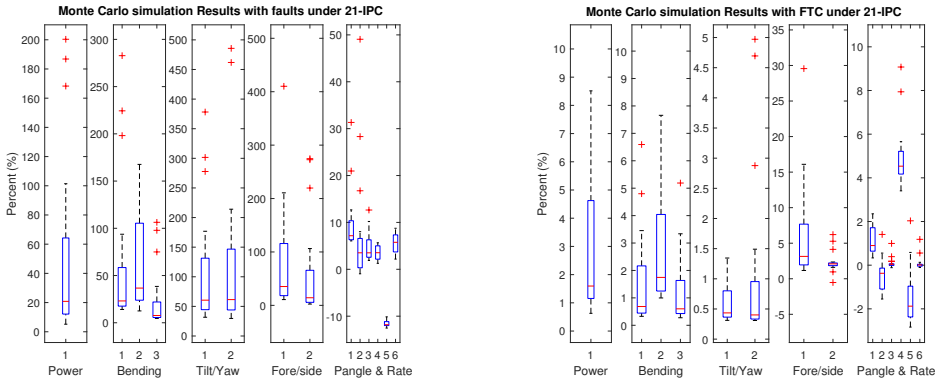

(a) With single pitch actuator LOSS fault (no FTC). (b) With single pitch actuator LOSS fault (with FTC).

Figure 12: Monte Carlo simulation results under 20 wind conditions with hub-height wind speed 21m/s with pitch actuator 2 suffering from the pitch loss fault

Furthermore, Fig.13 depicts the FE results of the pitch actuator with high air content fault and loss of effectiveness fault under one specific wind condition. It can be seen that the fault estimation can follow the actual pitch fault trajectory well. The magnitude of fault 2 is larger than that of fault 1. Accurate fault estimation is essential to guarantee fault-tolerance performance, which can avoid error propagation in the FE-based FTC scheme.

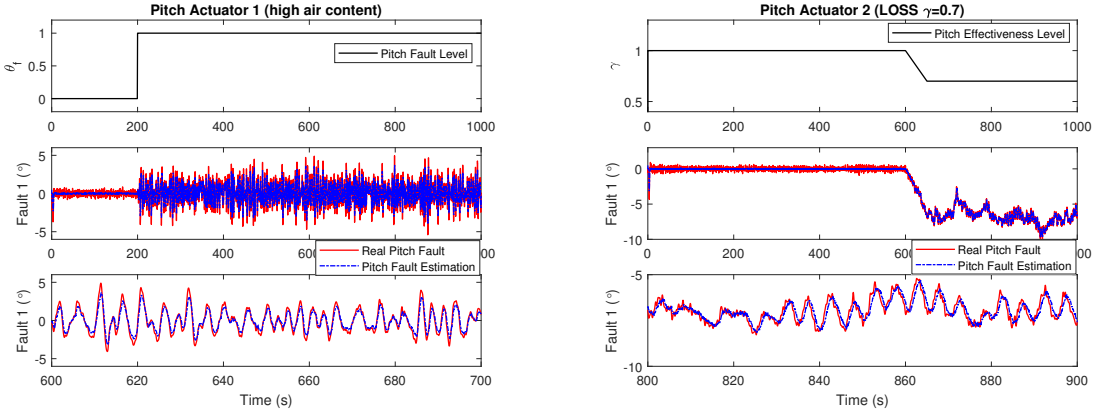

(a) Pitch actuator fault estimation in the one-fault case under L18-1 (b) Pitch actuator fault estimation in the one-fault case under L21-1

Figure 13: FE results

4.3. Multi-fault Case

Pitch actuator 1 is assumed to suffer from the hydraulic leakage fault f_1 during $[300, 500]s$, and at the same time pitch 2 suffers from the LOSS fault f_2 with $\gamma = 0.7$ within $[600, 1000]s$. Extensive simulation results conducted under the 40 wind conditions defined in Table.2 are presented.

To show the goodness of the FE computation, the *normalized root mean-squared error* (NRMSE) is used as the evaluation criterion, which varies between 0 to 1 (bad fit - perfect fit) as shown in (27). f denotes the pitch actuator fault, f_e is the corresponding fault estimation, *norm* indicates the 2-norm of the fault vector, and *mean* denotes the vector mean value. The NRMSE of FE results under different pitch controllers is shown in Table. 5.

$$NRMSE = 1 - (norm(f - f_e))/(norm(f - mean(f)) \tag{27}$$

Table 5
NRMSE of FE simulation results

Load Case	18 CPC_fault		18 IPC_fault		21 CPC_fault		21 IPC_fault	
	f_{1e}	f_{2e}	f_{1e}	f_{2e}	f_{1e}	f_{2e}	f_{1e}	f_{2e}
L1	0.64	0.90	0.51	0.83	0.59	0.94	0.46	0.84
L2	0.40	0.95	0.48	0.87	0.59	0.94	0.48	0.80
L3	0.64	0.92	0.48	0.84	0.62	0.92	0.44	0.83
L4	0.35	0.95	0.50	0.80	0.55	0.94	0.49	0.77
L5	0.55	0.94	0.47	0.87	0.58	0.94	0.47	0.83
L6	0.63	0.92	0.49	0.79	0.62	0.91	0.43	0.83
L7	0.44	0.95	0.49	0.84	0.25	0.96	0.50	0.87
L8	0.62	0.89	0.64	0.83	0.62	0.92	0.42	0.84
L9	0.64	0.91	0.50	0.83	0.44	0.95	0.50	0.74
L10	0.42	0.95	0.50	0.74	0.61	0.92	0.48	0.77
L11	0.61	0.93	0.48	0.81	0.60	0.93	0.45	0.83
L12	0.64	0.91	0.50	0.84	0.61	0.92	0.45	0.82
L13	0.64	0.91	0.50	0.78	0.55	0.94	0.46	0.87
L14	0.63	0.90	0.52	0.77	0.61	0.93	0.47	0.78
L15	0.63	0.90	0.52	0.82	0.60	0.93	0.48	0.75
L16	0.64	0.92	0.48	0.83	0.23	0.96	0.50	0.76
L17	0.63	0.92	0.48	0.81	0.30	0.96	0.50	0.84
L18	0.63	0.93	0.48	0.82	0.61	0.92	0.43	0.84
L19	0.64	0.92	0.49	0.79	0.61	0.93	0.43	0.85
L20	0.64	0.92	0.49	0.78	0.48	0.95	0.50	0.76
MIN	0.35	0.89	0.47	0.74	0.23	0.91	0.42	0.74
MAX	0.64	0.95	0.64	0.87	0.62	0.96	0.50	0.87
MEDIAN	0.62	0.93	0.49	0.83	0.59	0.93	0.47	0.83

From Table.5, it is interesting to note that the smaller the TI, the smaller the FE accuracy of the pitch actuator 1 fault f_1. This happens because f_1 is an incipient pitch fault with relatively small magnitude and the fault amplitude of f_1 becomes smaller when TI is lower. For a pitch actuator fault f_2, the FE accuracy presents negative correlation with wind TI. More importantly, the FE accuracy of f_2 is affected negatively by the large wind shear parameter. That is, when both the wind TI and shear are small, the FE performance improves, as expected. In other words the amplitude of f_2 itself is relatively large, when the wind TI and shear are both smaller, the standard deviation of pitch movements become smaller. Smooth pitch movements will achieve better fault FE results. Moreover, the FE accuracy of f_2 is always better than that of f_1. The FE performance of the load case L14 of 18IPC_fault (TI=0.204, Shear=0.246) is shown as Fig.14. It can be seen that the fault estimation can follow the real fault trajectory closely. An interaction exists between the dynamic effects of these two faults when TI is large, see [700-800]s of f_1 and [700-800]s of f_2.

Furthermore, the multiple pitch actuator fault effects and the corresponding FTC compensation performance in the frequency domain under wind condition L21_13 are depicted in Fig.15 and Fig.16, respectively. It is important to note that the 1P component (i.e. 0.2Hz) of flapwise bending moment 2 is mitigated by the proposed BO-based IPC in the fault-free case. In the IPC case, the multi-pitch actuator faults enhance the blade flapwise bending moment around 0.2Hz, while in the CPC case it slightly enhances the loading lower than 0.2Hz. Moreover, 0.2Hz of the tower fore-aft bending moment is enhanced due to the multi-faults both in the CPC and IPC case. Interestingly, the impact of multi-faults in the IPC case is slightly more severe compared to the CPC case. From Fig.16, it can be seen that the designed FTC can compensate the fault effects quite well, which attains the load mitigation under multiple pitch actuator faults. This implies that the accuracy of fault estimation is acceptable.

The Monte Carlo simulation results with multiple pitch actuator faults under 20 wind conditions with hub-height wind speed 18m/s are expressed in Fig.17. Table.6 provides the simulation results in terms of the median values of performance metrics. The influence of pitch actuator faults on the OWT performance can now be analyzed. Note that the power fluctuation and load performance have different degrees of enhancement, which is often more serious in the IPC case. Interestingly, the pitch angle fluctuations are enhanced, which indicates that the pitch actuator movements are restricted due to the incidence of faults. Meanwhile, the three pitch rate fluctuations are normally reduced which

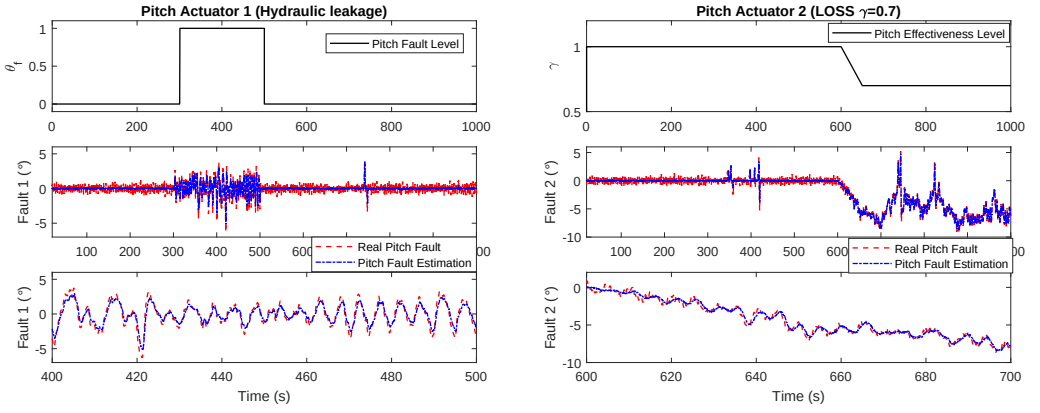

(a) Fault estimation of f_1 in the multi-fault case (b) Fault estimation of f_2 in the multi-fault case

Figure 14: FE results in load case L14 of 18IPC_fault, where the third subplot is part of the second subplot.

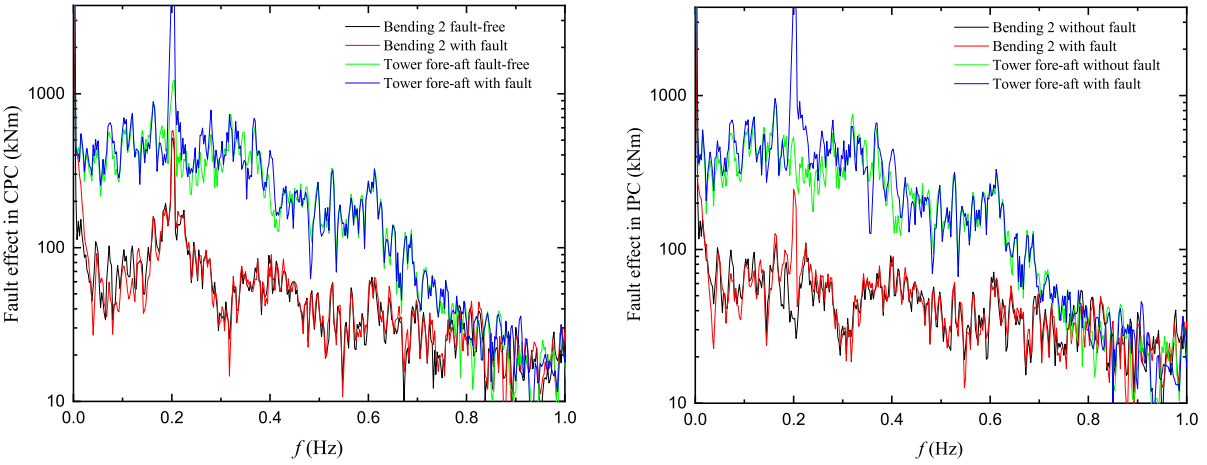

(a) CPC (b) IPC

Figure 15: Multiple pitch actuator fault effects in the frequency domain under wind condition L21_13.

reflects the couplings between three pitch actuators. Furthermore, the higher the performance, the more severe the fault effects. Last but not least, the effectiveness of the proposed FTC scheme is verified. It is noticeable that, in most cases, the OWT performance has been recovered to the corresponding fault-free case (using updated PI controller). Due to the interactions between two pitch fault dynamics, the OWT performance with FTC is a little lower than the fault-free case, which is still acceptable. Compared with the fault-free case with the original PI controller, the fault-tolerant IPC "co-design" scheme using BO can not only compensate the pitch actuator fault effects, but also achieve the reduction of power fluctuation, blade unbalanced loading fluctuation and pitch angle fluctuation. Therefore, the effectiveness and robustness of proposed actuator fault-tolerant wind turbine load mitigation control is verified.

5. Conclusion

This paper proposes a Bayesian optimization-based fault-tolerant IPC co-design strategy for OWT asymmetrical load mitigation with pitch actuator faults to reduce the rotor system fatigue and enhance sustainable operation. To enhance system robustness without having to use complex modelling the BO algorithm is adopted to search for the optimal PI pitch controller coefficients. The resulting FE-based UIO system is used within a combined FTC and load mitigation co-design to compensate the pitch actuator faults and restore good load mitigation performance. Monte

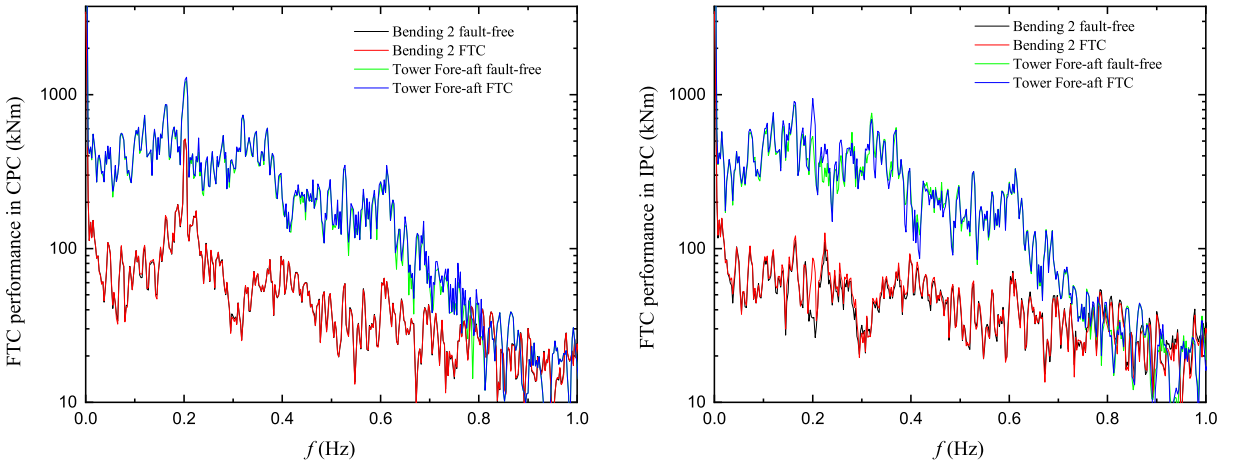

(a) CPC (b) IPC

Figure 16: FTC compensation performance in the frequency domain under wind condition L21_13.

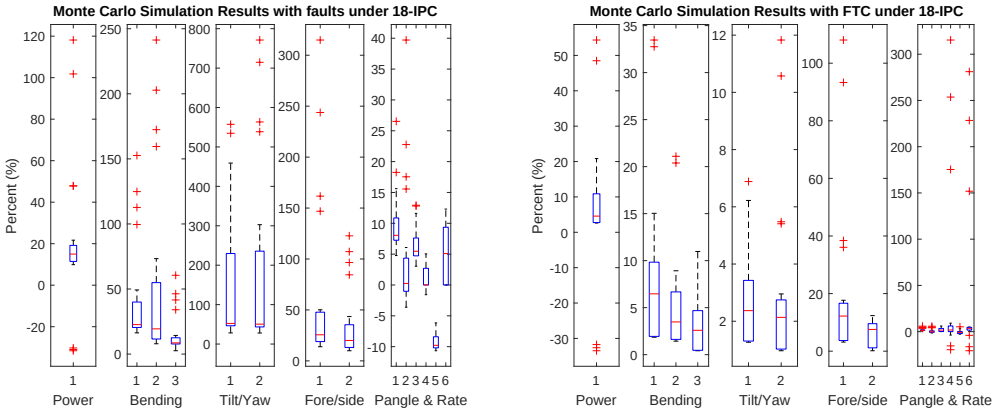

(a) With multiple pitch actuator faults (no FTC), namely 18IPC_fault.

(b) With multiple pitch actuator faults (with FTC), namely 18IPC_FTC.

Figure 17: Monte Carlo simulation results with updated PI-based CPC & IPC under 20 wind conditions with hub-height wind speed 18m/s

Carlo simulations have been performed on the 5MW NREL wind turbine with different wind conditions (different TI & shear parameters) and fault scenarios (single & multiple faults).

Simulation results indicate the effectiveness and robustness of the proposed "co-design" scheme. The proposed strategy can decease the generator power fluctuations and improve the load mitigation performance to a large extent in the fault-free case. The pitch activities are also reduced, which deceases the likelihood of pitch fault occurrence from the root. Meanwhile, good FE results and the ability of recovery to the fault-free level are impressing. It can be concluded that the proposed strategy presents significant improvement with respect to attain load mitigation performance both in healthy and faulty conditions. It can guarantee load mitigation performance in case of different pitch actuator faults through fault compensation. Moreover, the rotor aerodynamic asymmetries caused by the pitch faults are alleviated to the fault-free level.

Note that this scheme not only alleviates the power and blade unbalanced loading fluctuations, but also enhances the tolerance to the effects of potential pitch actuator faults. This strategy provides good load reduction and fault-tolerance using commonly used PI control with the added feature of fault estimation information that can have an important impact on O&M scheduling. The fault information is derived on-line and not using traditional condition monitoring.

Table 6
Median values of Simulation Results

Median	Power	Flap1	Flap2	Flap3	Tilt	Yaw	Fore	Side	Pangle1	Pangle2	Pangle3	Prate1	Prate2	Prate3
18CPC_PIVS	-48.19	-8.33	-8.25	-7.68	0.34	0.68	-21.30	8.15	-7.57	-7.57	-7.57	15.48	15.79	15.79
18IPC_PIVS	-48.30	-15.70	-15.20	-14.83	4.02	5.59	-22.30	-10.92	-8.31	-8.43	-8.45	-1.77	-9.87	-1.98
21CPC_PIVS	-45.41	-5.98	-5.01	-5.88	-0.12	-0.11	-17.80	1.79	-5.56	-5.56	-5.56	22.15	22.35	22.35
21IPC_PIVS	-45.78	-11.15	-11.63	-12.70	5.96	3.33	-18.46	-12.13	-6.32	-6.30	-6.02	-9.64	-9.63	-9.70
18CPC_fault	7.32	10.52	22.48	10.70	55.58	55.50	17.16	22.76	8.55	7.16	8.67	4.41	-3.10	6.57
18IPC_fault	14.99	22.63	19.38	8.60	52.34	50.49	25.59	20.04	8.05	0.25	5.47	0.01	-9.78	5.09
21CPC_fault	7.69	8.97	32.99	10.33	41.14	42.00	30.81	37.20	8.67	22.94	8.72	-2.86	-3.49	-9.30
21IPC_fault	18.72	28.74	38.32	9.45	67.19	67.77	45.67	17.11	7.71	3.78	5.26	-84.07	-11.93	-86.34
18CPC_FTC	2.02	0.17	0.19	0.13	0.11	-0.03	1.36	2.07	0.36	0.10	0.15	11.83	3.95	5.40
18IPC_FTC	4.58	6.47	3.48	2.59	2.37	2.14	8.18	7.55	1.42	-0.28	1.67	1.78	-0.77	3.59
21CPC_FTC	1.08	0.16	0.08	0.04	0.27	0.25	0.78	1.99	0.20	0.06	0.09	9.65	5.69	4.49
21IPC_FTC	2.64	3.43	2.20	0.81	9.98	7.01	5.55	4.99	2.36	-0.82	-0.18	-84.07	0.59	-86.34

The work has shown that the FTC and Load Mitigation problems are related in the sense that the latter is a system which is tolerant to adverse asymmetrical loading. The co-design combination of FTC and load mitigation is an important paradigm for sustainable OWT energy production with the prediction of reduced levelised cost of energy. Future work will include more realistic and complex fault scenarios under more wind scenarios, or directly using blade loading as different evaluation scores. Meanwhile, potential real physical experiments to verify the effectiveness of the proposed method is also included in the future work.

Acknowledgment

The authors would like to thank the UK EPSRC for funding support in the project "A New Partnership in Offshore Wind" through grant ref EP/R004900/1 [2017-2023], awarded to the Universities of Durham, Hull and Sheffield, as a Prosperity Partnership award led by Siemens-Gamesa.

A. Assumptions and Lemmas

Assumption 1. *(A, C) is observable, (A, B) is controllable. The control matching condition is satisfied for the actuator fault f_a with $rank(B, F_a) = rank(B)$, i.e. the actuator fault is matched.*

Assumption 2. *The fault f_a and disturbance d are norm-bounded. f_a has bounded first-order and second-order differentials.*

Remark 2. *The first part of Assumption 1 states some standard requirements for observer-based control systems, guaranteeing controllability of the system (16) and observability of the state and fault. The rank condition $rank(B, F_a) = rank(B)$ ensures that the fault f_a lies in the range space spanned by the control input u. Therefore, the fault f_a is matched and the fault effect on the system dynamics can be compensated through direct control actions. That is, they can be directly compensated by introducing their estimates into the control action. This so-called matching condition is one of the fundamental assumptions and prerequisites for realizing active fault compensation [47]. Assumption 2 implies that the fault f_a and disturbance d considered here are norm-bounded with unknown upper bounds, which is reasonable in practical applications. The existence of differentials is required for the UIO-based FE observer design.*

Lemma 1. *An error system with the following dynamics:*

$$\dot{e} = Ce + E_s d_s$$

is asymptotically stable with H_∞ performance $\|G_{ed_s}\|_\infty < \lambda$, which can be illustrated as:

$$J = \int_0^\infty (e^T e - \lambda^2 d_s^T d_s) dt < 0 \tag{28}$$

By defining a Lyapunov function $V = e_x^T P e_x$ with P is a symmetric positive definite matrix, and with assumed zero initial conditions, it holds that:

$$\begin{aligned} J &= \int_0^\infty (e^T e - \lambda^2 d_s^T d_s + \dot{V}) dt - \int_0^\infty \dot{V} dt \\ &= \int_0^\infty (e^T e - \lambda^2 d_s^T d_s + \dot{V}) dt - V(\infty) + V(0) \\ &\leq \int_0^\infty (e^T e - \lambda^2 d_s^T d_s + \dot{V}) dt \end{aligned}$$

One sufficient condition for (28) is illustrated as:

$$J_1 = e_y^T e_y - \lambda^2 w_d^T w_d + \dot{V} < 0$$

Lemma 2. *A system $\dot{x} = Ax$ is termed $\mathcal{D}$-stable if all its eigenvalues η of the state matrix A lie within the region $\mathcal{D}$. Assume $\mathcal{D}$ is a vertical strip region: $a_1 < Re(\eta_1) < b_1, a_1 < b_1 < 0$, the system $\dot{x} = Ax$ is $\mathcal{D}$-stable with the premise of existing a symmetric positive definite P_0 and satisfying the following LMI [48], where $\star$ represents the transpose of matrix elements in the symmetric position.*

$$\begin{bmatrix} He(P_0 A + A^T P_0) - 2b_1 P_0 & 0 \\ \star & -He(P_0 A + A^T P_0) + 2a_1 P_0 \end{bmatrix} < 0$$

References

[1] M DeCastro, S Salvador, M Gómez-Gesteira, X Costoya, D Carvalho, FJ Sanz-Larruga, and L Gimeno. Europe, China and the United States: Three different approaches to the development of offshore wind energy. *Renewable and Sustainable Energy Reviews*, 109:55–70, 2019.

[2] Michael Wilkinson, B Hendriks, F Spinato, K Harman, and etc. Gomez. Methodology and results of the reliawind reliability field study. In *European Wind Energy Conference and Exhibition*, volume 3, pages 1984–2004, 2010. Warsaw, April.

[3] Dale E Berg, Jose R Zayas, Donald W Lobitz, CP van Dam, Raymond Chow, and Jonathon P Baker. Active aerodynamic load control of wind turbine blades. In *Fluids Engineering Division Summer Meeting*, volume 42894, pages 1119–1127, 2007.

[4] EA Bossanyi. Individual blade pitch control for load reduction. *Wind Energy*, 6(2):119–128, 2003.

[5] EA Bossanyi. Further load reductions with individual pitch control. *Wind Energy*, 8(4):481–485, 2005.

[6] Torben Juul Larsen, Helge A Madsen, and Kenneth Thomsen. Active load reduction using individual pitch, based on local blade flow measurements. *Wind Energy: An International Journal for Progress and Applications in Wind Power Conversion Technology*, 8(1):67–80, 2005.

[7] Kausihan Selvam, Stoyan Kanev, Jan Willem van Wingerden, Tim van Engelen, and Michel Verhaegen. Feedback–feedforward individual pitch control for wind turbine load reduction. *International Journal of Robust and Nonlinear Control: IFAC-Affiliated Journal*, 19(1):72–91, 2009.

[8] Alexander Stotsky and Bo Egardt. Individual pitch control of wind turbines: Model-based approach. *Proceedings of the Institution of Mechanical Engineers, Part I: Journal of Systems and Control Engineering*, 227(7):602–609, 2013.

[9] GAM Van Kuik, Joachim Peinke, Rogier Nijssen, Denja Lekou, Jakob Mann, Jens Nørkær Sørensen, Carlos Ferreira, Jan-Willem van Wingerden, David Schlipf, Pieter Gebraad, et al. Long-term research challenges in wind energy–a research agenda by the european academy of wind energy. *Wind energy science*, 1(1):1–39, 2016.

[10] Jianshen Li and Shuangxin Wang. Dual multivariable model-free adaptive individual pitch control for load reduction in wind turbines with actuator faults. *Renewable Energy*, 174:293–304, 2021.

[11] Karl A Stol, Wenxin Zhao, and Alan D Wright. Individual blade pitch control for the controls advanced research turbine (CART). *Solar Energy Engineering*, 128(4):498–505, 2006.

[12] E Bossanyi, A Wright, and P Fleming. Controller field tests on the NREL CART2 turbine, tech. rep. nrel/tp-5000-49085. Technical report, National Renewable Energy Lab.(NREL), Golden, CO (United States), 2010.

[13] Ervin Bossanyi, Paul Fleming, and Alan Wright. Field test results with individual pitch control on the NREL CART3 wind turbine. In *50th AIAA Aerospace Sciences Meeting including the New Horizons Forum and Aerospace Exposition*, pages 1019–1028, 2012.

[14] Martin Shan, Jörn Jacobsen, and Steffen Adelt. Pitch control systems for a 5 MW offshore wind turbine. In *EE-S Conference*, 2013. Bremen, May 13-15.

[15] Ervin A Bossanyi, Paul A Fleming, and Alan D Wright. Validation of individual pitch control by field tests on two-and three-bladed wind turbines. *IEEE Transactions on Control Systems Technology*, 21(4):1067–1078, 2013.

[16] Edwin van Solingen, Paul A Fleming, Andrew Scholbrock, and Jan-Willem van Wingerden. Field testing of linear individual pitch control on the two-bladed controls advanced research turbine. *Wind Energy*, 19(3):421–436, 2016.

[17] Daniel Ossmann, Peter Seiler, Christopher Milliren, and Alan Danker. Field testing of multi-variable individual pitch control on a utility-scale wind turbine. *Renewable Energy*, 170:1245–1256, 2021.

[18] Xiaoxu Liu, Zhiwei Gao, and Michael ZQ Chen. Takagi–sugeno fuzzy model based fault estimation and signal compensation with application to wind turbines. *IEEE Transactions on Industrial Electronics*, 64(7):5678–5689, 2017.

[19] Jianglin Lan, Ron J Patton, and Xiaoyuan Zhu. Fault-tolerant wind turbine pitch control using adaptive sliding mode estimation. *Renewable Energy*, 116:219–231, 2018.

[20] Hamed Badihi, Youmin Zhang, Pragasen Pillay, and Subhash Rakheja. Fault-tolerant individual pitch control for load mitigation in wind turbines with actuator faults. *IEEE Transactions on Industrial Electronics*, 68(1):532–543, 2020.

[21] Yichao Liu, Joeri Frederik, Riccardo MG Ferrari, Ping Wu, Sunwei Li, and Jan-Willem van Wingerden. Fault-tolerant individual pitch control of floating offshore wind turbines via subspace predictive repetitive control. *Wind Energy*, 24(9):1045–1065, 2021.

[22] Yashar Mousavi, Geraint Bevan, and Ibrahim Beklan Kucukdemiral. Fault-tolerant optimal pitch control of wind turbines using dynamic weighted parallel firefly algorithm. *ISA transactions*, 2021.

[23] Zhiwei Gao and Xiaoxu Liu. An overview on fault diagnosis, prognosis and resilient control for wind turbine systems. *Processes*, 9(2):300, 2021.

[24] Yashar Mousavi, Geraint Bevan, and Ibrahim Beklan Kucukdemiral. Fault-tolerant optimal pitch control of wind turbines using dynamic weighted parallel firefly algorithm. *ISA transactions*, 128:301–317, 2022.

[25] Peter Fogh Odgaard, Héctor Sánchez, Teresa Escobet, and Vicenç Puig. Fault diagnosis and fault tolerant control with application on a wind turbine low speed shaft encoder. *IFAC-PapersOnLine*, 48(21):1357–1362, 2015.

[26] Hamed Badihi and Youmin Zhang. Fault-tolerant individual pitch control of a wind turbine with actuator faults. *IFAC-PapersOnLine*, 51(24):1133–1140, 2018.

[27] Jianglin Lan and Ron J Patton. A new strategy for integration of fault estimation within fault-tolerant control. *Automatica*, 69:48–59, 2016.

[28] Alexander Stotsky. Blade root moment sensor failure detection based on multibeam LiDAR for fault-tolerant individual pitch control of wind turbines. *Energy Science & Engineering*, 2(3):107–115, 2014.

[29] Yanhua Liu, Ron J Patton, and Jianglin Lan. Fault-tolerant individual pitch control using adaptive sliding mode observer. *IFAC Safeprocess.*, 51(24):1127–1132, 2018. Warsaw, Aug.

[30] Yanhua Liu, Ron J Patton, and Shuo Shi. Wind turbine asymmetrical load reduction with pitch sensor fault compensation. *Wind Energy*, 23(7):1523–1541, 2020.

[31] Eric Brochu, Vlad M Cora, and Nando De Freitas. A tutorial on Bayesian optimization of expensive cost functions, with application to active user modeling and hierarchical reinforcement learning. *arXiv preprint arXiv:1012.2599*, 2010.

[32] Carl Edward Rasmussen and Christopher KI Williams. Gaussian processes for machine learning. 2006. *The MIT Press, Cambridge, MA, USA*, 38:715–719, 2006.

[33] Jason Jonkman, Sandy Butterfield, Walter Musial, and George Scott. Definition of a 5-MW reference wind turbine for offshore system development. *National Renewable Energy Laboratory, Golden, CO, Technical Report No. NREL/TP-500-38060*, 2009.

[34] Richie Gao and Zhiwei Gao. Pitch control for wind turbine systems using optimization, estimation and compensation. *Renewable Energy*, 91:501–515, 2016.

[35] Yanhua Liu, Ron J Patton, and Shuo Shi. Asymmetrical load mitigation of wind turbine pitch actuator faults using unknown input-based fault-tolerant control. *IFAC World Congress 2020*, 2020. Berlin, 12-17 July.

[36] Peter I Frazier. A tutorial on Bayesian optimization. *arXiv preprint arXiv:1807.02811*, 2018.

[37] Jonathan Ko and Dieter Fox. GP-BayesFilters: Bayesian filtering using Gaussian process prediction and observation models. *Autonomous Robots*, 27(1):75–90, 2009.

[38] Andrew Wilson and Ryan Adams. Gaussian process kernels for pattern discovery and extrapolation. In *International Conference on Machine Learning*, pages 1067–1075, 2013. Atlanta, June.

[39] Charles George Broyden. The convergence of a class of double-rank minimization algorithms 1. general considerations. *IMA Journal of Applied Mathematics*, 6(1):76–90, 1970.

[40] Niranjan Srinivas, Andreas Krause, Sham M Kakade, and Matthias W Seeger. Information-theoretic regret bounds for gaussian process optimization in the bandit setting. *IEEE Transactions on Information Theory*, 58(5):3250–3265, 2012.

[41] Peter Fogh Odgaard, Jakob Stoustrup, and Michel Kinnaert. Fault tolerant control of wind turbines–a benchmark model. *IFAC Proceedings Volumes*, 42(8):155–160, 2009.

[42] Ganesh R Naik. *Advances in Principal Component Analysis: Research and Development*. Springer Singapore, 2017. https://doi.org/10.1007/978-981-10-6704-4.

[43] Hamed Habibi, Hamed Rahimi Nohooji, and Ian Howard. Adaptive PID control of wind turbines for power regulation with unknown control direction and actuator faults. *IEEE Access*, 6:37464–37479, 2018.

[44] Jie Chen, Ron J Patton, and Hong-Yue Zhang. Design of unknown input observers and robust fault detection filters. *International Journal of control*, 63(1):85–105, 1996.

[45] Stephen Boyd, Laurent El Ghaoui, Eric Feron, and Venkataramanan Balakrishnan. *Linear matrix inequalities in system and control theory*, volume 15. Siam, 1994.

[46] Bonnie J Jonkman. Turbsim user's guide: Version 1.50. 2009.

[47] Jianglin Lan and Ron J Patton. A decoupling approach to integrated fault-tolerant control for linear systems with unmatched non-differentiable faults. *Automatica*, 89:290–299, 2018.

[48] Mahmoud Chilali and Pascal Gahinet. H/sub/spl infin//design with pole placement constraints: an LMI approach. *IEEE Transactions on automatic control*, 41(3):358–367, 1996.

Yanhua Liu received the B.Eng., M.Eng.degrees in Automation department from the North China Electric Power University, China, in 2012 and 2015, respectively. She achieved her Ph.D. degree in Control & Intelligent Systems Engineering Research Group, University of Hull, in 2019. From 2019 to 2021, She worked as a postdoc in the project "A New Partnership in Offshore Wind", Department of Engineering, University of Hull. She is currently a Lecturer with the School of Electrical Engineering, Shandong University, Jinan, China. Her research interests lie in the power electronics, offshore wind turbine, wave energy and model predictive control.

Ron J. Patton was born in Peru in 1949. He graduated at Sheffield University with BEng, MEng and PhD degrees in Electrical & Electronic Engineering and Control Systems, in 1971, 1974, and 1980, respectively. He currently holds the Chair in Control & Intelligent Systems Engineering at Hull University. He has made a substantial contribution to the field of modelling and design of robust methods for Fault Detection and Isolation (FDI) and Fault tolerant Control (FTC) in dynamic systems as author of 376 papers, including 138 journal papers and 6 books. His research interests are: Robust, multiple-model and de-centralized control strategies for FTC systems and FTC methods for renewable energy. He is Life Fellow of IEEE, Senior Member of AIAA and Fellow of the Institute of Measurement and Control.

Shuo Shi was born in Shandong, China. He received the M.Eng. degree in Automation department from the North China Electric Power University, P.R. China, in 2016. He achieved his Ph.D. degree in Control & Intelligent Systems Engineering Research Group, University of Hull, in 2022. Ongoing research interests lie in the wave energy optimal control, wave estimation and prediction.